Real-time Optimization of Gear Shift Trajectories using Quadratic Programming for Electric Vehicles with Dual Clutch Transmission

Taeheon Lee and Seibum B. Choi, Member, IEEE

***Abstract*—The main focus of this paper is a method for real-time optimization of the gear shift trajectories for electric vehicles (EVs) with dual clutch transmissions. First, a driveline model was arranged for each gear shift process. The states in each gear shift process can be predicted through these models. An objective function is composed of a frequency-shaped jerk to minimize the shift shock and take into account the bandwidth limit of the lower-level controller. Equality constraints are defined for smooth model changes during the gear shift processes. Moreover, the conditions needed to reflect the driver's pedal input (which can be changed in real-time) is composed of an equality constraint. In addition, inequality constraints are constructed to limit the maximum value of the torque, torque rate, and jerk during gear shift processes. Finally, the problem is formulated in quadratic programming (QP) form. The gear shift trajectories and feedforward inputs are generated by obtaining an optimal solution through the QP solver. The performance of the proposed algorithm is verified through testbench experiments.**

***Index Terms*—Gear shift trajectory planning, Real-time optimization, Feedforward input, Quadratic programming, Dual clutch transmission, Electric vehicles.**

I. Introduction

THE automobile industry has been dominated chiefly by internal combustion (IC) engine vehicles. However, as fuel efficiency and carbon emission regulations have tightened globally in recent years, demand for energy-efficient hybrid and electric vehicles has rapidly increased. The automobile industry is entering a new phase. In the future, the proportion of hybrid and electric vehicles in the automobile market is expected to increase [1]. Furthermore, there is a forecast that EVs no longer need a transmission. Until now, most EVs using a reducer have been released, and Porsche's taycan and Audi's e-Tron GT are the only EVs equipped with a two-speed transmission. Since both vehicles are sports cars, they are equipped with transmissions designed to achieve high torque performance at low speeds rather than focusing on the vehicle's energy efficiency. However, the EV with a reducer is insufficient to satisfy the tightened regulations, and transmission is needed to increase energy efficiency and maximize the performance of the motor [2]–[4]. Specifically, [5] and [6] claim that transmission in an EV will increase the energy efficiency in various driving cycles by operating the motor for a long time in a high energy efficiency section. Transmission with a small number of stages is required to increase energy efficiency and maximize the performance and durability of the motor in EVs [5], [6]. Therefore, the demand for dual clutch transmissions (DCTs), which have no torque interruption during gear shifting and have high energy transmission efficiency, in EV is expected to continue.

Gear shift control is essential for vehicles with a transmission. The most critical point in the gear shift control is eliminating shift shock to improve the driver's ride quality. In particular, unlike an automatic transmission (AT), a DCT does not have a torque converter that absorbs the shift shock [7]. Thus, a more precise gear shift control is required in the DCT.

Many types of research have been conducted on gear shift control. In [8], gear shift control was classified into two phases (torque phase and inertia phase). The gear shift was performed by creating shift trajectories for each phase and tracking them. Various trajectory tracking controllers were proposed in [9] and [10]. On the other hand, standardized trajectories were used in the gear shift process [9]–[11]. However, quantitative analysis for the trajectories was not performed at all. To change the standardized trajectory shape, the output shaft torque trajectory (which can be changed according to the gear shift time) was used in [12]. In [13], a polynomial trajectory was introduced. Various shapes of the trajectory could be implemented according to their order. However, there was the limitation that the trajectory of [12] and [13] were not analyzed through the driveline model. Meanwhile, conditions for reducing lockup oscillation were introduced through model analysis in [14]. Furthermore, many types of research were conducted to optimize the gear shift control using a model. In [15], the gear shift control was performed to minimize jerk in the inertia phase. In [16], a control allocation method was proposed to distribute the input values optimally during the gear shift process. In [17] and [18], an objective function was constructed using the weighted sum of various physical quantities such as slip, friction work, and differential values of the clutch torque. Gear shift control was achieved through a linear quadratic regulator (LQR) control method using the objective function. However, this has the disadvantage that it cannot accommodate the limit of the hardware input. Thus, gear shift control methods applying a model predictive control (MPC) technique were proposed in [19] and [20] to overcome these limitations. However, because [19] and [20] only dealt with control in the inertia phase, they could not treat the situation when the phase changes. In [21], an optimization problem was studied that considers the model change for all gear shift processes, and gear shift trajectories were created through

T.Lee and S.B.Choi (Corresponding author) are the Korea Advanced Institute of Science and Technology, 291, Daehak-ro Yuseong-gu, Daejeon, 34141, South Korea (e-mail: pos99126@kaist.ac.kr, sbchoi@kaist.ac.kr).

nonlinear programming. Due to the limitations of nonlinear programming, real-time application of the algorithm is not possible, and it cannot cope with various initial conditions and situations of gear shifting.

In this paper, first, a real-time optimization algorithm of the gear shift trajectory is proposed for parallel hybrid and electric vehicles that can cope with a variety of situations. Frequency-shaped jerk is used as the objective function to reduce the shift shock and consdier the lower-level controller bandwidth. Additionally, constraints are proposed to consider the smooth model changes in each gear shift process and limits of the motor and clutch torques. For real-time optimization, all models and constraints are linear form, and the optimization problem can be constructed as a QP form. Thus, the solutions can be found using a QP solver. The gear shift trajectories are generated using the optimal solutions. From this process, the motor's fast and precise torque control performance can be actively utilized for entire gear shift control through prediction and optimization. Second, the driver's pedal input is considered an equality constraint when constructing the optimization problem. The driver can input the desired torque command to the vehicle through the pedal. The driver's pedal input may change in real-time according to vehicle status, traffic conditions, and driver characteristics. The vehicle's acceleration cannot be controlled directly according to the driver's pedal input during the gear shift process, because there are other targets to control. However, if the endpoint of the gear shift trajectory is designed considering the driver's pedal input, the driver can achieve drivability immediately after gear shifting. This is another advantage of optimizing the gear shift trajectory in real-time.

This paper is organized as follows. Section 2 describes the control-oriented model of the driveline and explains the gear shift process and trajectory. In addition, the model is arranged in the state-space form according to the gear shift phases, which is used for the trajectory optimization in Section 3. Section 3 proceeds with state prediction using the model. After that, an objective function, equality constraints, and inequality constraints are constructed to generate gear shift trajectories. The optimization problem is transformed into QP form, and an optimal solution is obtained using a QP solver. Finally, gear shift trajectories are generated using the optimal solution. Section 4 provides verification of the performance of the real-time optimization algorithm through testbench experiments. Section 5 consists of a conclusion that summarizes the contents of this paper.

II. Driveline model and gear shift process

Section 2 briefly describes the control-oriented model and the gear shift process. First, a general control-oriented model of the driveline is introduced. Then, explanations about each gear shift process and general gear shift trajectories are introduced. After that, the control-oriented model is arranged in a state-space form according to each gear shift phase. The arranged model is used in the optimization algorithm for the gear shift trajectory.

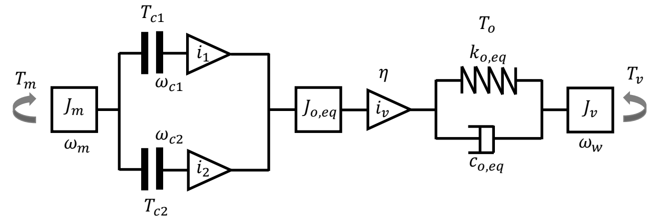

Fig. 1: Control-oriented model of the driveline

A. Control-oriented model

Fig. 1 shows a control-oriented model of the driveline. It consists of a low-order model and expresses the driveline's transmission efficiency. A detailed description of how the model was configured is in [22]. In this paper, the dynamic equations for Fig. 1 are briefly introduced.

In Fig. 1, the torque balance equation of the motor and the clutch is as follows.

$$T_m - T_{c1} - T_{c2} = J_m \dot{\omega}_m \tag{1}$$

$$T_{c1} = \begin{pmatrix} T_m - J_m\dot{\omega}_m - T_{c2} & (Engaged) \\ \mu_{k,c1} r_{c1} N_{c1} F_{c1} & (Slipping) \\ 0 & (Disengaged) \end{pmatrix} \tag{2}$$

$$T_{c2} = \begin{pmatrix} T_m - J_m\dot{\omega}_m - T_{c1} & (Engaged) \\ \mu_{k,c2} r_{c2} N_{c2} F_{c2} & (Slipping) \\ 0 & (Disengaged) \end{pmatrix} \tag{3}$$

where T_m, T_{c1}, T_{c2}, J_m, and ω_m are motor torque, clutch 1 torque, clutch 2 torque, lumped inertia from the motor to the clutch, and motor speed. The terms μ_k, r, N, and F represent the dynamic friction coefficient of the clutch, effective radius of the clutch, the number of the clutch plate, and the clutch actuator force. The subscript $c1$ and $c2$ mean the clutch 1 and clutch 2. (1) shows the torque balance equation of the motor. (2) and (3) represent the clutch 1 and 2 torque according to the state of the clutch.

$$(T_{c1} i_1 + T_{c2} i_2)\,\eta - T_o = J_{o,eq}\eta \frac{\dot{\omega}_{c1}}{i_1} \tag{4}$$

$$\dot{T}_o = c_{o,eq}\left(\frac{\dot{\omega}_{c1}}{i_1} - \dot{\omega}_w\right) + k_{o,eq}\left(\frac{\omega_{c1}}{i_1} - \omega_w\right) \tag{5}$$

$$T_o - T_v = J_v \dot{\omega}_w \tag{6}$$

where T_o, T_v, ω_{c1}, ω_w, i_1, i_2, i_v, and J_v are output shaft torque, external resistance torque, speed of the clutch 1, speed of the wheel, the gear ratio of first gear, the gear ratio of second gear, the gear ratio of the virtual gear, and lumped vehicle inertia. The value of i_v is 1, and the gear is a virtual gear representing the driveline's lumped transmission efficiency. Here, η means the energy transmission efficiency of the virtual gear. η is used to express the transmission loss in the actual driveline. The terms $J_{o,eq}$, $k_{o,eq}$, and $c_{o,eq}$ are the lumped inertia from the clutch to the output shaft, equivalent torsional stiffness, and equivalent torsional damping coefficient. (4) shows the torque balance equation with driveline transmission efficiency. (5) is the compliance model of the output shaft and (6) is the dynamics of the wheel and vehicle inertia. (5) is constructed to represent the resonance frequency of the driveline.

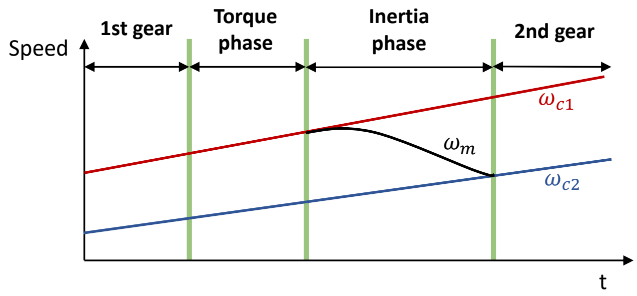

(a)

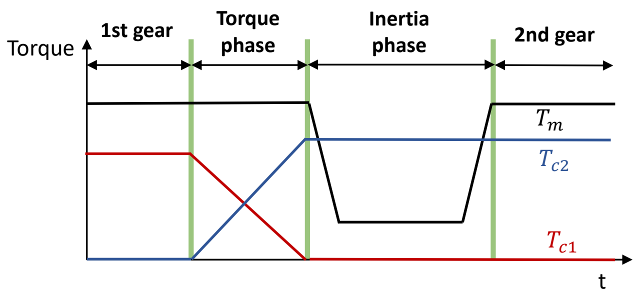

(b)

Fig. 2: Gear shift trajectories: (a) Speed trajectories of each driveline component. (b) Torque trajectories of each driveline component.

B. Gear shift process and state-space model in each gear shift phase

The gear shift of the DCT is divided into upshift and downshift. Since the two processes are inverted, only the upshift is dealt with in this paper. The upshift from 1st to 2nd gear proceeds in the order: 1st gear, torque phase, inertia phase, and 2nd gear. The torque phase represents the process in which the power transmitted from clutch 1 is transferred to clutch 2. Clutch 1 is entirely disengaged at the end of the torque phase. When clutch 1 is disengaged, the inertia phase starts. The inertia phase is the process in which the speeds of the motor and clutch 2 are synchronized. When the speeds of the motor and clutch 2 are synchronized, the upshift is completed, and 2nd gear starts. Fig. 2 shows the speed and torque trajectories for each gear shift phase [10]. In the torque phase of Fig. 2b, the power transmitted from clutch 1 is transferred to clutch 2. In the inertia phase of Fig. 2a, the speed of the motor and clutch 2 are synchronized. By tracking the slip and torque trajectories shown in Fig. 2, it is possible to play a role in each gear shift phase.

Here, the model is arranged into a state-space form for each gear shift phase. Because the gear shift proceeds for a short time ($\sim 1s$), it can be assumed that T_v is constant during the gear shift.

$$\dot{T}_v = 0 \tag{7}$$

In addition, the lower-level torque controller of the motor and the clutch 2 can be described as first order dynamics as follows.

$$\dot{T}_m = -a_1 T_m + a_1 T_{m,cmd} \tag{8}$$

$$\dot{T}_{c2} = -a_2 T_{c2} + a_2 T_{c2,cmd} \tag{9}$$

where $T_{m,cmd}$ and $T_{c2,cmd}$ are command of the motor torque and command of the clutch 2 torque. Here, a_1 and a_2 represent the bandwidth of the motor and clutch 2 controllers. For the testbench, it is modeled as $a_1 = 2\pi{\cdot}4$ and $a_2 = 2\pi{\cdot}4$. This may be changed depending on the device and the characteristics of the lower-level controller.

The filtered output shaft torque signal can also be expressed in state-space form, (10).

$$\begin{aligned} \dot{x}_{aux} &= A_w x_{aux} + B_w T_o \\ y_{aux} &= C_w x_{aux} + D_w T_o \end{aligned} \tag{10}$$

where x_{aux} and y_{aux} are the auxiliary state of the filter and the output state of the filter. The terms A_w, B_w, C_w, and D_w are the matrices when the filter is expressed in state-space form. The input of the filter is output shaft torque in (10). A detailed description of the above filter is given in Section 3.

The driveline model can be arranged to state-space form according to each gear shift phase. First, the characteristics of each phase are described as follows. In 1st gear, clutch 1 is engaged and clutch 2 is disengaged. In the torque phase, clutch 1 is engaged and clutch 2 is slipping. In the inertia phase, clutch 1 is disengaged and clutch 2 is slipping. In 2nd gear, clutch 1 is disengaged and clutch 2 is engaged. Inputs for each phase are set to $\dot{T}_{m,cmd}$ and $\dot{T}_{c2,cmd}$. In addition, 1st and 2nd gear models are used only for prediction without additional inputs. The model can be arranged as (11) considering the above contents. The detailed descriptions of A_1, A_{TP}, A_{IP}, A_2, B_{TP}, and B_{IP} in (11) are summarized in the Appendix.

(11) can be discretized using the zero-order hold equivalent method. The sampling time of discretization (T_s) is $0.01s$. The equation is as follows.

$$x\left(k+1\right) = \bar{A}_{phase,d} x\left(k\right) + \bar{B}_{phase,d} u\left(k\right) \tag{12}$$

where the subscript d indicates a discrete system. The subscript $phase$ is replaced by $1st$, TP, IP, $2nd$ according to each gear shift phase. The terms $\bar{A}_{1,d}$, $\bar{A}_{TP,d}$, $\bar{A}_{IP,d}$, $\bar{A}_{2,d}$, $\bar{B}_{TP,d}$, and $\bar{B}_{IP,d}$ are discretized matrix of $\bar{A}_1$, $\bar{A}_{TP}$, $\bar{A}_{IP}$, $\bar{A}_2$, $\bar{B}_{TP}$, and $\bar{B}_{IP}$. (12) is used to generate gear shift trajectories in Section 3.

III. Real-time optimization of the gear shift trajectories

In this section, a real-time optimization algorithm is proposed to generate the gear shift trajectory using the model. Since the model must be switched according to the gear shift phase, the conditions must be satisfied for smooth model switching. Therefore, a prediction for the entire gear shift phase should be required to use the above conditions. As the prediction horizon increases, the size of the optimization problem increases. From this, the amount of computation needed to solve optimization problems also increases. To satisfy the computational time, the sampling time of the trajectory optimization algorithm (T_{s1}) was set to $100ms$.

A. Overview of a trajectory optimization algorithm

Fig. 3 shows the optimization problem for the gear shift trajectory when the shift flag is entered. Fig. 3 represents the predicted trajectory of the state over time. The initial

$$\left\{\begin{array}{ll} \dot{x}=\bar{A}_1 x=\begin{bmatrix} A_1 & \mathbf{0} \\ B_w C_3 & A_w \end{bmatrix} x, \quad y_{aux}=\bar{C}_1 x=\begin{bmatrix} D_w C_3 & C_w \end{bmatrix} x & (1st\,gear) \\ \dot{x}=\bar{A}_{TP} x+\bar{B}_{TP} u=\begin{bmatrix} A_{TP} & \mathbf{0} \\ B_w C_3 & A_w \end{bmatrix} x+\begin{bmatrix} B_{TP} \\ \mathbf{0} \end{bmatrix} u, \quad y_{aux}=\bar{C}_{TP} x=\begin{bmatrix} D_w C_3 & C_w \end{bmatrix} x & (torque\,phase) \\ \dot{x}=\bar{A}_{IP} x+\bar{B}_{IP} u=\begin{bmatrix} A_{IP} & \mathbf{0} \\ B_w C_3 & A_w \end{bmatrix} x+\begin{bmatrix} B_{IP} \\ \mathbf{0} \end{bmatrix} u, \quad y_{aux}=\bar{C}_{IP} x=\begin{bmatrix} D_w C_3 & C_w \end{bmatrix} x & (inertia\,phase) \\ \dot{x}=\bar{A}_2 x=\begin{bmatrix} A_2 & \mathbf{0} \\ B_w C_3 & A_w \end{bmatrix} x, \quad y_{aux}=\bar{C}_2 x=\begin{bmatrix} D_w C_3 & C_w \end{bmatrix} x & (2nd\,gear) \end{array}\right.$$

$$\begin{aligned} where \quad x &= \begin{pmatrix} x_1 & x_2 & x_3 & x_4 & x_5 & x_6 & x_7 & x_8 & \vdots & x_{aux} \end{pmatrix}^T \\ &= \begin{pmatrix} \omega_m-\omega_{c2} & \frac{\omega_{c2}}{i_2}-\omega_w & T_o & T_m & T_{m,cmd} & T_{c2} & T_{c2,cmd} & T_v & \vdots & x_{aux} \end{pmatrix}^T \\ u &= \begin{pmatrix} u_1 & u_2 \end{pmatrix}^T = \begin{pmatrix} \dot{T}_{m,cmd} & \dot{T}_{c2,cmd} \end{pmatrix}^T, \quad C_3=\begin{bmatrix} 0 & 0 & 1 & 0 & 0 & 0 & 0 & 0 \end{bmatrix} \end{aligned} \tag{11}$$

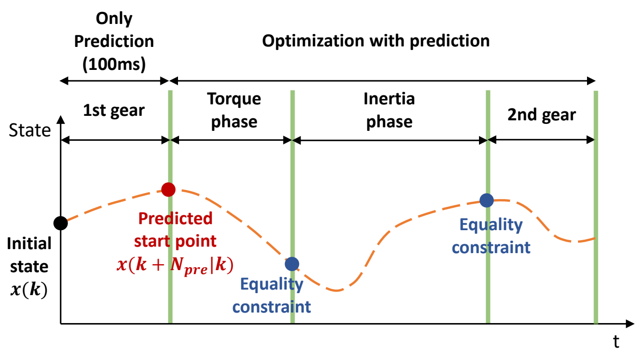

Fig. 3: Predicted trajectory of the state over time.

values of the states are measured using a sensor or estimated using a state observer [22]–[26]. Future states can be predicted depending on the model and input values. As mentioned above, the sampling time of the optimization algorithm (T_{s1}) is $100ms$. Therefore, the actual powertrain states move to a value other than the current states for T_{s1}. The states prediction after T_{s1} is used with the 1st gear model to compensate for these differences. The predicted states after T_{s1} are defined as predicted start points. After that, the optimization problem for the gear shift trajectory is constructed by setting the corresponding point as the starting point of the optimization section.

The model changes four times (1st gear, torque phase, inertia phase, and 2nd gear) during the gear shift process. The duration of each model is defined as t_{pre}, t_{TP}, t_{IP}, and t_{2nd}. The meaning of the above parameters and how to set the values are as follows. t_{pre} means the time of the interval to predict the state change during the sampling time of the algorithm. Therefore, it must be set equal to the sampling time of the optimization algorithm. In addition, t_{TP} and t_{IP} mean the duration of torque phase and inertia phase. The values of t_{TP} and t_{IP} depend on the physical characteristics of the driveline. Depending on the inertia value of the power source and vehicle, and the torque and torque rate limits of each input, the t_{TP} and t_{IP} values that can perform gear shifting are changed. t_{TP} and t_{IP} values must be properly set so that the optimization problem defined in the later section forms a feasible problem. If the values are set too small, the problem always becomes infeasible. In this case, the values must be increased. On the other hand, if the values are set excessively large, the gear shift time becomes too long, resulting in poor results. Usually, in a general sense of the gear shift control, t_{TP} should be set smaller than t_{IP}. t_{TP} and t_{IP} values must be set through the trial and error method considering the above contents. Finally, since t_{2nd} is a value required to observe the lockup oscillation, it is desirable to set it to a value enough to observe the oscillation In this paper, corresponding values are set to $t_{pre} = 0.1s$, $t_{TP} = 0.3s$, $t_{IP} = 0.6s$, $t_{2nd} = 0.2s$. Therefore, the parameters indicating the number of discrete steps in each phase are $N_{pre} = t_{pre}/T_s$, $N_{TP} = t_{TP}/T_s$, $N_{IP} = t_{IP}/T_s$, $N_{2nd} = t_{2nd}/T_s$. In addition, the upshift process always proceeds in the order of 1st gear, torque phase, inertia phase, and 2nd gear. Future states can be predicted using this relationship, and the optimization problem can be constructed.

B. Optimization problem formulation

a) State prediction: Future states can be predicted using the appropriate model for each phase [27], [28]. Prediction from the initial step to $(N_{pre} + N_{TP} + N_{IP} + N_{2nd})\,th$ step must be performed. It is assumed that $k = 0$ when the shift flag is first entered. The initial state prediction should be defined in the case of $k = 0$. However, to simplify the description of the overall algorithm, it is better to generalize and indicate it as a state prediction for the kth step. Therefore, the explanation about state prediction at the $0th$ step proceeds, but the notation is indicated as the kth step.

Suppose that any y satisfies the equation $y(k) = \bar{C}x(k)$ in (12). If the shift flag is entered, the predicted start point can be predicted as follows.

$$y\left(k+N_{pre}|k\right)=\bar{C}A_{1,d}^{N_{pre}}x\left(k\right) \quad \cdots \; 1st\,gear \tag{13}$$

where $y\left(k+N_{pre}|k\right)$ represents predicted states of the $(k+N_{pre})\,th$ step predicted in the kth step.

State prediction during the gear shift is possible in the same way. Because the number of steps in the torque and inertia phase is $N_{TP} + N_{IP}$, the input sequence is from $u(0)$ to

$$
\begin{gathered}
Y=\bar{F}x\left(k+N_{pre}|k\right)+\bar{\Phi}U \\
Y=\left[\begin{array}{c}
y\left(k+N_{pre}+1|k\right) \\
y\left(k+N_{pre}+2|k\right) \\
\vdots \\
y\left(k+N_{pre}+N|k\right) \\
y\left(k+N_{pre}+N+1|k\right) \\
\vdots \\
y\left(k+N_{pre}+N_{last}|k\right)
\end{array}\right],\ \bar{F}=\left[\begin{array}{c}
\bar{C}\bar{A}_{TP,d} \\
\bar{C}\bar{A}_{TP,d}^{2} \\
\vdots \\
\bar{C}\bar{A}_{TP,d}^{N} \\
\bar{C}\bar{A}_{TP,d}^{N+1} \\
\vdots \\
\bar{C}\bar{A}_{2,d}^{N_{2nd}}\bar{A}_{IP,d}^{N_{IP}}\bar{A}_{TP,d}^{N_{TP}}
\end{array}\right],\ U=\left[\begin{array}{c}
u\left(0\right) \\
u\left(N\right) \\
\vdots \\
u\left(N_{TP}+N_{IP}-N\right)
\end{array}\right] \\
\bar{\Phi}=\left[\begin{array}{cccc}
\bar{C}\bar{B}_{TP,d} & 0 & \cdots & 0 \\
\bar{C}\left(\bar{A}_{TP,d}+I\right)\bar{B}_{TP,d} & 0 & \cdots & 0 \\
\vdots & \vdots & \cdots & 0 \\
\bar{C}\left(\sum\limits_{i=1}^{N-1}\bar{A}_{TP,d}^{i-1}\right)\bar{B}_{TP,d} & 0 & \cdots & 0 \\
\bar{C}\bar{A}_{TP,d}\left(\sum\limits_{i=1}^{N}\bar{A}_{TP,d}^{i-1}\right)\bar{B}_{TP,d} & \bar{C}\bar{B}_{TP,d} & \cdots & 0 \\
\vdots & \vdots & \vdots & \vdots \\
\bar{\Phi}_{N_{last},1} & \bar{\Phi}_{N_{last},2} & \cdots & \bar{\Phi}_{N_{last},(N_{TP}+N_{IP})/N}
\end{array}\right],\ N_{last}=N_{TP}+N_{IP}+N_{2nd} \\
\bar{\Phi}_{N_{last},1}=\bar{C}\bar{A}_{2,d}^{N_{2nd}}\bar{A}_{IP,d}^{N_{IP}}\bar{A}_{TP,d}^{N_{TP}-N}\left(\sum_{i=1}^{N}\bar{A}_{TP,d}^{i-1}\right)\bar{B}_{TP,d},\ \bar{\Phi}_{N_{last},2}=\bar{C}\bar{A}_{2,d}^{N_{2nd}}\bar{A}_{IP,d}^{N_{IP}}\bar{A}_{TP,d}^{N_{TP}-2N}\left(\sum_{i=1}^{N}\bar{A}_{TP,d}^{i-1}\right)\bar{B}_{TP,d} \\
\bar{\Phi}_{N_{last},(N_{TP}+N_{IP})/N}=\bar{C}\bar{A}_{2,d}^{N_{2nd}}\left(\sum_{i=1}^{N}\bar{A}_{IP,d}^{i-1}\right)\bar{B}_{IP,d}
\end{gathered}
\tag{14}
$$

$u(N_{TP}+N_{IP}-1)$. Therefore, the total number of independent inputs is $2\cdot(N_{TP}+N_{IP})$. As the number of input sequences increases, the time required to solve the optimization problem greatly increases. The number of input sequences must be reduced to ensure real-time operation of optimization. The following assumptions are used to reduce the number of input sequences. For every N step, the value of each input sequence is the same. It can be expressed as follows.

$$
\begin{aligned}
& u_1\left(Nj\right)=u_1\left(Nj+1\right)=\cdots=u_1\left(Nj+N-1\right) \\
& u_2\left(Nj\right)=u_2\left(Nj+1\right)=\cdots=u_2\left(Nj+N-1\right) \\
& \quad where \quad (j=0,1,\cdots,(N_{TP}+N_{IP})/N-1)
\end{aligned}
\tag{15}
$$

It should be noted that N_{TP} and N_{IP} must be set to multiples of N.

By applying (15), the state prediction from the predicted start point to $(k+N_{pre}+N_{TP}+N_{IP}+N_{2nd})\,th$ step is as (14).

In addition, the derivative of state prediction can be defined as follows.

$$
\Delta y\left(k+i+1|k\right)=\left(y\left(k+i+1|k\right)-y\left(k+i|k\right)\right)/T_s \tag{16}
$$

Similarly, the derivative of state prediction from the predicted start point to $(k+N_{pre}+N_{TP}+N_{IP}+N_{2nd})\,th$ step is as (17). From (14) and (17), both Y and ΔY can be expressed as a linear combination of the predicted start point $x\left(k+N_{pre}|k\right)$ and the input sequence U. By properly setting the $\bar{C}$ value, all predicted states in the form of (14) and (17) can be used to construct objective funciton, equality constraints, and inequality constraints.

b) Objective function: Shift shock causes discomfort to the driver. The shift shock can be defined through a physical quantity called a jerk, which is a derivative of the vehicle acceleration. The vehicle acceleration is proportional to the output shaft torque of the driveline. Therefore, jerk can be defined through output shaft torque. In [29] and [30], it is noted that most drivers can feel a jerk of $10m/s^3$ or more, making the ride very uncomfortable. In addition, it depends on the person, but some drivers could feel a jerk of $3-6m/s^3$. Therefore, the gear shift trajectory with a small jerk value must be generated so that the driver cannot feel the shift shock at all. Thus, the objective function must be constructed using Δx_3. Additionally, the gear shift trajectory is a target value that the lower-level controller must track. Because there is a bandwidth limit in the lower-level controller, it is good to create the trajectory considering its control performance. Therefore, the gear shift trajectory is preferred as a combination of low-frequency components.

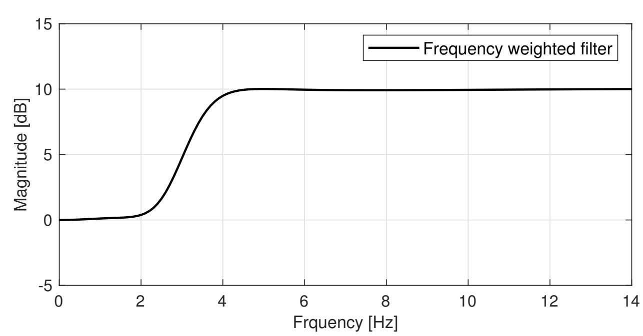

Fig. 4: Frequency weighted filter.

$$\Delta Y = \Delta \bar{F} x\left(k+N_{pre}|k\right) + \Delta\bar{\Phi} U$$

$$\Delta Y = \begin{bmatrix} \Delta y\left(k+N_{pre}+1|k\right) \\ \Delta y\left(k+N_{pre}+2|k\right) \\ \vdots \\ \Delta y\left(k+N_{pre}+N|k\right) \\ \Delta y\left(k+N_{pre}+N+1|k\right) \\ \vdots \\ \Delta y\left(k+N_{pre}+N_{last}|k\right) \end{bmatrix},\ \Delta\bar{F} = \begin{bmatrix} \bar{C}\Delta\bar{A}_{TP,d} \\ \bar{C}\Delta\bar{A}_{TP,d}\bar{A}_{TP,d} \\ \vdots \\ \bar{C}\Delta\bar{A}_{TP,d}\bar{A}_{TP,d}^{N-1} \\ \bar{C}\Delta\bar{A}_{TP,d}\bar{A}_{TP,d}^{N} \\ \vdots \\ \bar{C}\Delta\bar{A}_{2,d}\bar{A}_{2nd,d}^{N_{2nd}-1}\bar{A}_{IP,d}^{N_{IP}}\bar{A}_{TP,d}^{N_{TP}}, \end{bmatrix},\ U = \begin{bmatrix} u(0) \\ u(N) \\ \vdots \\ u\left(N_{TP}+N_{IP}-N\right) \end{bmatrix}$$

$$\bar{\Phi} = \begin{bmatrix} \bar{C}\bar{B}_{TP,d} & 0 & \cdots & 0 \\ \bar{C}\left(\bar{A}_{TP,d}+I\right)\bar{B}_{TP,d} & 0 & \cdots & 0 \\ \vdots & \vdots & \cdots & 0 \\ \bar{C}\left(\sum_{i=1}^{N-1}\bar{A}_{TP,d}^{i-1}\right)\bar{B}_{TP,d} & 0 & \cdots & 0 \\ \bar{C}\bar{A}_{TP,d}\left(\sum_{i=1}^{N}\bar{A}_{TP,d}^{i-1}\right)\bar{B}_{TP,d} & \bar{C}\bar{B}_{TP,d} & \cdots & 0 \\ \vdots & \vdots & \vdots & \vdots \\ \bar{\Phi}_{N_{last},1} & \bar{\Phi}_{N_{last},2} & \cdots & \bar{\Phi}_{N_{last},(N_{TP}+N_{IP})/N} \end{bmatrix},\ N_{last} = N_{TP}+N_{IP}+N_{2nd}$$

$$\begin{aligned} &\Delta\bar{\Phi}_{N_{last},1} = \bar{C}\Delta\bar{A}_{2,d}\bar{A}_{2,d}^{N_{2nd}-1}\bar{A}_{IP,d}^{N_{IP}}\bar{A}_{TP,d}^{N_{TP}-N}\left(\sum_{i=1}^{N}\bar{A}_{TP,d}^{i-1}\right)\bar{B}_{TP,d} \\ &\Delta\bar{\Phi}_{N_{last},2} = \bar{C}\Delta\bar{A}_{2,d}\bar{A}_{2,d}^{N_{2nd}-1}\bar{A}_{IP,d}^{N_{IP}}\bar{A}_{TP,d}^{N_{TP}-2N}\left(\sum_{i=1}^{N}\bar{A}_{TP,d}^{i-1}\right)\bar{B}_{TP,d} \\ &\Delta\bar{\Phi}_{N_{last},(N_{TP}+N_{IP})/N} = \bar{C}\Delta\bar{A}_{2,d}\bar{A}_{2,d}^{N_{2nd}-1}\left(\sum_{i=1}^{N}\bar{A}_{IP,d}^{i-1}\right)\bar{B}_{IP,d},\ \Delta\bar{A}_{1,d} = \left(\bar{A}_{1,d}-I\right)/T_s,\ \Delta\bar{A}_{TP,d} = \left(\bar{A}_{TP,d}-I\right)/T_s, \\ &\Delta\bar{A}_{IP,d} = \left(\bar{A}_{IP,d}-I\right)/T_s,\ \Delta\bar{A}_{2,d} = \left(\bar{A}_{2,d}-I\right)/T_s,\ \Delta\bar{B}_{TP,d} = \bar{B}_{TP,d}/T_s,\ \Delta\bar{B}_{IP,d} = \bar{B}_{IP,d}/T_s \end{aligned} \tag{17}$$

Fig. 4 shows a high pass filter with a magnitude of $0dB$ from 0 to $2Hz$ and $10dB$ from 4 to $inf Hz$. The filter is applied to the output shaft torque value to give frequency weighting. It acts as a penalty function in the objective function. (10) represents the state-space form of Fig. 4.

The objective function used to minimize the shift shock and accommodate the bandwidth limit of the lower-level controller is as follows.

$$J = \sum_{i=1}^{N_{TP}+N_{IP}+N_{2nd}} \Delta y_{aux}^2\left(k+N_{pre}+i|k\right) \tag{18}$$

$\Delta y_{aux}\left(k+N_{pre}+i|k\right)$ means the predicted derivative of the output shaft torque shaped in the frequency domain. It has the same meaning as the frequency-shaped jerk in the objective function. Frequency-shaped jerks during 2nd gear are included in (18). These reduce the lockup oscillation that occurs after the gear shift is complete. Since the frequency-shaped jerks during 2nd gear are included in the objective function, the condition to reduce lockup oscillation noted in [14] does not need to be added as an additional constraint.

c) Equality constraints: When the model is changed, the conditions for smooth model switching are expressed as an equality constraint. First, when it goes from torque phase to inertia phase, the clutch 1 must be released when the clutch 1 torque is zero. Clutch 1 toque in the torque phase can be represented as the sum of the other states in (2). Thus, the following constraints are constructed.

$$\begin{gathered} \bar{C}_{Tc1}x\left(k+N_{pre}+N_{TP}|k\right) = 0 \\ where\ \ C_{Tc1} = \left[\begin{matrix} 0 & 0 & \frac{J_m}{\left(J_m+J_{o,eq}/i_1^2\right)i_1\eta} & \frac{J_{o,eq}/i_1^2}{\left(J_m+J_{o,eq}/i_1^2\right)} \end{matrix}\right. \\ \left.\begin{matrix} 0 & \frac{-\left(J_{o,eq}/i_1^2+J_m i_2/i_1\right)}{\left(J_m+J_{o,eq}/i_1^2\right)} & 0 & 0 & \vdots & \mathbf{0} \end{matrix}\right] \end{gathered} \tag{19}$$

Second, when it goes from the inertia phase to the 2nd gear, the slip between the motor and clutch 2 must be zero to complete the gear shift. A corresponding condition is necessary for model switching. Additionally, to obtain fast drivability when 2nd gear engages, the motor torque at the end of the inertia phase must match the driver's desired torque value. The above two conditions can be expressed as follows.

$$\begin{aligned} x_1\left(k+N_{pre}+N_{TP}+N_{IP}|k\right) &= 0 \\ x_4\left(k+N_{pre}+N_{TP}+N_{IP}|k\right) &= g\left(\varphi(k)\right) \end{aligned} \tag{20}$$

where $g(\varphi)$ is a function representing the desired torque value proportional to the pedal input, and $\varphi(k)$ means the driver's pedal input at kth step.

d) Inequality constraints: Since the driver feels the maximum jerk, the instantaneous jerk should not exceed a specific value during the gear shifting process. Moreover, even after the gear shift is completed, the jerk caused by lockup oscillation must not exceed a specific value. Due to the difference between the model and the plant, jerks greater than the expected value may occur as a lockup oscillation. For this reason, the baseline of jerk is set conservatively for the 2nd gear period. Therefore, the inequality constraints for instantaneous jerks are divided into two sections. They are represented as follows.

$$\begin{gathered} -jerk_{\max} \leq \Delta x_3 \left(k+N_{pre}+i|k\right) \cdot r_{eff}/J_v \leq jerk_{\max} \\ where \quad (i=1,2,\cdots,N_{TP}+N_{IP}) \\ -jerk_{\max,2} \leq \Delta x_3 \left(k+N_{pre}+i|k\right) \cdot r_{eff}/J_v \leq jerk_{\max,2} \\ where \quad (i=N_{TP}+N_{IP}+1,\cdots,N_{TP}+N_{IP}+N_{2nd}) \end{gathered} \tag{21}$$

where r_{eff}, J_v, $jerk_{max}$, and $jerk_{max,2}$ are the effective radius of the wheel, vehicle inertia, maximum jerk limit for the torque phase and the inertia phase, and the maximum jerk limit for the 2nd gear.

In addition, the clutch 1 and 2 torque values during the torque phase should always be greater than zero. This can be expressed as follows.

$$\begin{gathered} x_7\left(k+N_{pre}+i|k\right) \geq 0 \quad (i=1,2,\cdots,N_{TP}) \\ \bar{C}_{Tc1} x\left(k+N_{pre}+i|k\right) \geq 0 \quad (i=1,2,\cdots,N_{TP}) \end{gathered} \tag{22}$$

To make a monotonic decreasing slip trajectory in the inertia phase, the derivative of the slip must always be less than ε. It can be expressed as follows.

$$\Delta x_1\left(k+N_{pre}+i|k\right) \leq \varepsilon \quad (i=N_{TP}+1,\cdots,N_{TP}+N_{IP}) \tag{23}$$

where ε means the maximum slope of the slip.

Finally, the motor torque during the gear shift must have a value between the limits. The clutch torque during the inertia phase should be greater than the lower limit. The input rate of the motor and the clutch 2 should also have a value bewteen the limits. These are represented as follows.

$$\begin{gathered} T_{m,\min} \leq x_5\left(k+N_{pre}+i|k\right) \leq T_{m,\max} \\ where \quad (i=1,2,\cdots,N_{TP}+N_{IP}) \\ T_{c2,\min} \leq x_7\left(k+N_{pre}+i|k\right) \\ where \quad (i=N_{TP}+1,N_{TP}+2,\cdots,N_{TP}+N_{IP}) \\ \begin{bmatrix} \dot{T}_{m,\min} \\ \dot{T}_{c2,\min} \end{bmatrix} \leq u\left(j\right) \leq \begin{bmatrix} \dot{T}_{m,\max} \\ \dot{T}_{c2,\max} \end{bmatrix} \\ where \quad (j=0,N,\cdots,(N_{TP}+N_{IP}-N_{IP,step})-N) \\ \begin{bmatrix} \dot{T}_{m,\min 1} \\ \dot{T}_{c2,\min 1} \end{bmatrix} \leq u\left(j\right) \leq \begin{bmatrix} \dot{T}_{m,\max 1} \\ \dot{T}_{c2,\max 1} \end{bmatrix} \\ where \quad (j=N_{TP}+N_{IP}-N_{IP,step},\cdots, \\ (N_{TP}+N_{IP})-N) \end{gathered} \tag{24}$$

where $T_{m,min}$, $T_{m,max}$, $T_{c2,min}$, $\dot{T}_{m,min}$, $\dot{T}_{m,max}$, $\dot{T}_{c2,min}$, and $\dot{T}_{c2,max}$ are the minimum and maximum limits of the motor torque, the minimum limits of the clutch 2 torque, the minimum and maximum limits of the motor torque rate, and the minimum and maximum limits of the clutch 2 torque rate. $\dot{T}_{m,min1}$, $\dot{T}_{m,max1}$, $\dot{T}_{c2,min1}$, and $\dot{T}_{c2,max1}$ represent the minimum and maximum limits of the motor torque rate, and the minimum and maximum limits of the clutch 2 torque rate for $N_{IP,step}$ steps. $N_{IP,step}$ is the number of steps before the end of the inertia phase, and it must be set to a multiple of N. The reason for dividing the section is that there is always a difference between the plant and model. Therefore, there is a possibility that the gear shift ends earlier than expected due to slip control errors in the actual plant. In this case, unexpected large lockup oscillation may occur if the motor and clutch torque do not reach the desired values. To prevent this phenomenon, the motor and clutch 2 torque trajectories should be reached near the desired value before $N_{IP,step}$ step ahead from the end of the inertia phase. For that reason, each section is divided in two as in (24). $\dot{T}_{m,min1}$, $\dot{T}_{m,max1}$, $\dot{T}_{c2,min1}$, and $\dot{T}_{c2,max1}$ must be set to a lower value than $\dot{T}_{m,min}$, $\dot{T}_{m,max}$, $\dot{T}_{c2,min}$, and $\dot{T}_{c2,max}$.

C. QP formulation

(18) is converted as follows by (17).

$$\begin{aligned} J &= \Delta Y^T \Delta Y \\ &= U^T \Delta\bar{\Phi}^T \Delta\bar{\Phi} U + 2x^T\left(k+N_{pre}|k\right) \Delta\bar{F}^T \Delta\bar{\Phi} U \\ &\quad + x^T\left(k+N_{pre}|k\right) \Delta\bar{F}^T \Delta\bar{F} x\left(k+N_{pre}|k\right) \end{aligned} \tag{25}$$

All equality constraints have the form $\bar{C}x\left(k+N_{pre}+i|k\right) = c_{eq} \quad (i=1,\ \cdots,\ N_{TP}+N_{IP})$. Therefore, the left side of the equality constraints can be expressed as the ith row of Y. To select the ith row of Y, the H_i is defined as a matrix with a size of $1 \times (N_{TP}+N_{ip}+N_{2nd})$. All elements of H_i are 0 except for the ith column, and the value of the ith column of H_i is 1. Then, each equality constraint satisfies the following expression.

$$\begin{gathered} \bar{C}x\left(k+N_{pre}+i|k\right) = H_i\bar{F}x\left(k+N_{pre}|k\right) + H_i\bar{\Phi}U = c_{eq} \\ \Leftrightarrow H_i\bar{\Phi}U = c_{eq} - H_i\bar{F}x\left(k+N_{pre}|k\right) \end{gathered} \tag{26}$$

All inequality constraints have the form $\bar{C}x\left(k+N_{pre}+i|k\right) \leq c_{ineq1}$ and $\bar{C}\Delta x\left(k+N_{pre}+i|k\right) \leq c_{ineq2}$ $(i=1,\cdots,\ N_{TP}+N_{IP}+N_{2nd})$. Similarly, each inequality constraint satisfies the following expression.

$$\begin{aligned} &\bar{C}x\left(k+N_{pre}+i|k\right) \\ &\qquad = H_i\bar{F}x\left(k+N_{pre}|k\right) + H_i\bar{\Phi}U \leq c_{ineq1} \\ &\qquad \Leftrightarrow H_i\bar{\Phi}U \leq c_{ineq1} - H_i\bar{F}x\left(k+N_{pre}|k\right) \\ &\bar{C}\Delta x\left(k+N_{pre}+i|k\right) \\ &\qquad = H_i\Delta\bar{F}x\left(k+N_{pre}|k\right) + H_i\Delta\bar{\Phi}U \leq c_{ineq2} \\ &\qquad \Leftrightarrow H_i\Delta\bar{\Phi}U \leq c_{ineq2} - H_i\Delta\bar{F}x\left(k+N_{pre}|k\right) \end{aligned} \tag{27}$$

By (25), (26), and (27), the objective function, all equality constraints, and all inequality constraints are converted to QP form for the input sequence U. The optimization problem for the gear shift trajectory can be rearranged to a general QP form through the above processes. (28) shows the general QP form.

$$\begin{gathered} \min\ \tfrac{1}{2}U^TQU + f^TU \\ s.t.\ A_{ineq}U \leq b_{ineq},\ A_{eq}U = b_{eq},\ Q > 0 \end{gathered} \tag{28}$$

In this case, the QP solver is applied to obtain an optimal solution. In this paper, QPOASES is used as the QP solver [31], [32].

Algorithm 1 A real-time optimization algorithm of the gear shift trajectory

Input: $x(k)$, $u^*(k - N_{iter}, 1 : N_{pre}/N)$, $\varphi(k)$.
Output: $x_{ref}(k, 1 : N_{iter})$, $u^*(k, 1 : N_{pre}/N)$.
Initialization : set N_{pre}, N_{TP}, N_{IP}, N_{2nd}, $k = 0$, $N_{iter} = 10\ (T_{s1}/T_s)$, N, $N_{IP,step}$, $constraints$.

if $k = 0$ **then**
  $x\left(k + N_{pre}|k\right) \leftarrow \bar{A}_{1,d}^{N_{pre}} x\left(k\right)$
  $N_{TP,now} \leftarrow N_{TP}, \;\; N_{IP,now} \leftarrow N_{IP}$
  configure QP problem using (19)-(25), $N_{TP,now}$, and $N_{IP,now}$
else
  if $k \leq N_{TP} - N_{iter}$ **then**

$$x\left(k + N_{pre}|k\right) \leftarrow \bar{A}_{TP,d}^{N_{pre}} x\left(k\right) + \sum_{i=1}^{\frac{N_{pre}}{N}} \bar{A}_{TP,d}^{N_{pre}-Ni} \cdot \left(\bar{A}_{TP,d}^{N-1} + \cdots + I\right) \bar{B}_{TP,d} u^*\left(k - N_{iter}, i\right)$$

    $N_{TP,now} \leftarrow N_{TP} - k, \;\; N_{IP,now} \leftarrow N_{IP}$
    configure QP problem using (19)-(25), $N_{TP,now}$, and $N_{IP,now}$
  else

$$x\left(k + N_{pre}|k\right) \leftarrow \bar{A}_{IP,d}^{N_{pre}} x\left(k\right) + \sum_{i=1}^{\frac{N_{pre}}{N}} \bar{A}_{IP,d}^{N_{pre}-Ni} \cdot \left(\bar{A}_{IP,d}^{N-1} + \cdots + I\right) \bar{B}_{IP,d} u^*\left(k - N_{iter}, i\right)$$

    $N_{TP,now} \leftarrow 0, \;\; N_{IP,now} \leftarrow N_{IP} - \left(k - N_{TP}\right)$
    configure QP problem using (20), (21), (23), (24), (25), $N_{TP,now}$, and $N_{IP,now}$
  end if
end if
solve U^* using QPOASES [31]
compute $x_{ref}\left(k, 1 : N_{iter}\right)$ using $x\left(k + N_{pre}|k\right)$ and U^*.
update $x_{ref}\left(k, 1 : N_{iter}\right)$ and $u^*\left(k, 1 : N_{pre}/N\right)$
$k \leftarrow k + N_{iter}$

D. Optimization algorithm sequence for the gear shift trajectories

A real-time optimization algorithm of the gear shift trajectories is performed every $100ms$. The contents noted in Section 2 and 3 show the process of constructing the optimization problem when the shift flag is entered. As the gear shift process progresses, the N_{TP}, the N_{IP} values must be changed. The optimization problems must be constructed to account for the change of N_{TP} and N_{IP} values over time. Thus, new parameters $N_{TP,now}$ and $N_{IP,now}$ are used in the algorithm to indicate the change of N_{TP} and N_{IP} values. The method of constructing a new optimization problem over time is shown through the algorithm 1.

The sampling time of the optimization algorithm (T_{s1}) is $100ms$, but the sampling time of the lower-level controller (T_s) is $10ms$. To generate a gear shift trajectory with the sampling time of T_s, the gear shift trajectory must be output in the size of $n \times N_{iter}$. Here, n means the size of state vector x. The output $x_{ref}\left(k, 1 : N_{iter}\right)$ are trajectories to be tracked by the lower-level controller. In addition, $u^*\left(k, 1 : N_{pre}/N\right)$ is another output. $u^*\left(k, 1 : N_{pre}/N\right)$ is used as an input value for calculating the predicted start point of the optimization algorithm in the next step. To match the sampling time of the algorithm (T_{s1}), k is changed in the unit of N_{iter}.

IV. Experimental Results

A. Experimental set-up and sceario

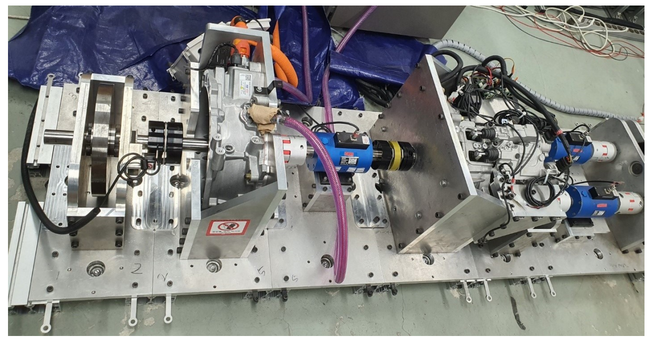

Fig. 5: Testbench configuration.

Fig. 5 shows the actual configuration of the testbench. It depicts the powertrain of an electric vehicle with a DCT. The components of the testbench are as follows. The power source is a motor. Power generated from the motor is transmitted through a dual clutch and corresponding gear (1st or 2nd gear). The normal forces pressing each clutch are controlled through each linear actuator and diaphragm, and the number of the gear stage (1st or 2nd) is determined by which clutch is engaged. The rear parts of the testbench consist of the output shaft, which describes the vehicle's drive shaft, and the vehicle inertia plate, which describes the vehicle mass. The testbench can be described through the control-oriented model in Fig. 1. The parameter values for the control-oriented model of the testbench are summarized in Tab. I. In addition, encoders are installed to measure the speed of the motor and each clutch, and wheel. In addition, torque sensors are installed behind the motor and each clutch for verification. The sampling rate of each sensor is $10ms$. The testbench is controlled using a microautobox2 and laptop. To solve the QP problem proposed in Section 3, QPOASES is implemented as a QP solver.

The overall structure of the gear shift control is shown in Fig. 6. When the shift flag is entered, the gear shift starts. The optimization algorithm is performed to generate gear shift trajectories using the initial states and the driver's pedal input. Because the torque sensor is not installed in the production

TABLE I: Model parameters of the testbench

Parameter	Value	Parameter	Value
J_m	0.27	$k_{o,eq}$	22000
$J_{o,eq}$	2.6	$c_{o,eq}$	185
J_v	144.5	i_1	15.38
r_{eff}	0.31	i_2	8.33
η	0.92		

Units are SI derived(kg, m, s)

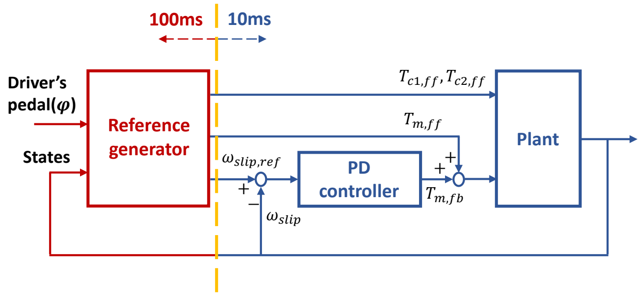

Fig. 6: Overall structure of the gear shift control logic in the inertia phase.

TABLE II: Tuning parameters of Algorithm 1

Symbol	Value	Symbol	Value
N	5	$\dot{T}_{m,min}$	-500
$N_{IP,step}$	5	$\dot{T}_{m,min}$	500
$jerk_{max}$	3	$\dot{T}_{c2,min}$	-120
$jerk_{max,2}$	1	$\dot{T}_{c2,max}$	120
ε	-2	$\dot{T}_{m,min1}$	-40
$T_{m,min}$	1	$\dot{T}_{m,max1}$	40
$T_{m,max}$	70	$\dot{T}_{c2,min1}$	-40
$T_{c2,min}$	0	$\dot{T}_{c2,max1}$	40

vehicle, the initial states have to be estimated using a torque observer [22]–[26]. However, this paper is focused only on verifying the performance of the gear shift trajectory. Thus, the value of the initial states is obtained using the torque sensors in the testbench experiment. Real-time optimization of the gear shift trajectory is done through Algorithm 1. The tuning parameters of the algorithm used in the experiment are shown in Tab. II. The optimization algorithm generates the trajectory and feedforward inputs, but using these alone is not enough to control the actual plant. Disturbances such as friction and unmodeled dynamics exist in an actual plant. Since the model is somewhat accurate, the value of the disturbance is not expected to be large. However, suppose that only the feedforward control is applied to the actual plant. In this case, the actual slip value does not exactly go to zero, especially in the inertia phase, resulting in a situation in which the gear shift is not completed. At this time, the clutch is continuously slipping, which generates frictional energy loss. Thus, it can significantly shorten the life of the clutch. Therefore, the lower-level controller aims to track slip trajectory and eliminate the steady-state errors of the slip even for unmodeled dynamics and disturbances. In the torque phase, the lower-level controller consists of feedforward control only. In the inertia phase, the lower-level controller consists of feedforward and feedback control. The feedforward control uses the feedforward inputs calculated using the optimization algorithm. The feedback control consists of a PD controller to track the slip trajectory accurately in the inertia phase. Thus, as shown in Fig. 6, the slip controller in the inertia phase uses both feedforward and feedback control.

There are three experimental scenarios. The first scenario is a situation in which the gear shift occurs when a constant driver's pedal input is applied. It is desired to analyze the shape of the trajectories generated from the proposed algorithm. It is for comparison with the conventional gear shift trajectories. The second scenario is when the driver releases the pedal during the gear shift. Similarly, the gear shift is performed using the proposed algorithm, and we would like to analyze the shape of the trajectories. For the above two scenarios, we would like to compare the change in the shape of the trajectories. The third scenario is when the driver presses the pedal during the gear shift. This scenario is designed to compare the difference between the proposed algorithm and the conventional method that did not reflect the pedal input in real time. For a horizontal comparison, it is set to have the same gear shift time. We would like to compare the results of the two methods in terms of drivability and maximum jerk.

B. Experimental results

In the testbench experiment, the maximum computation time of the optimization algorithm is about $20ms$. Thus, it can sufficiently run at a sampling time of $100ms$. Fig. 7 shows the experimental results for the first scenario. Fig. 7a shows the speed trajectory and measurements of each component, Fig. 7b shows the torque trajectoreis and measurements of each component, Fig. 7c shows the output shaft torque trajectory and measurements, and Fig. 7d shows the driver's desired motor torque value. The torque phase is from 41.1 to $41.4s$, and the inertia phase is from 41.4 to $42s$. The dashed line represents the reference trajectories from the proposed algorithm. The solid line shows measured values of the testbench experiments. In particular, the solid black line in Fig. 7b has higher frequency components than other measurements. Because of the location where the torque sensor is installed, the actual T_m value cannot be measured directly. Therefore, the compensated value ($T_{measured} + J_m\dot{\omega}_m$) was plotted to obtain the actual T_m value. In this process, high-frequency noises are added from the derivative term of the rotational speed. In addition, in Fig. 7c, it can be seen that the measured output torque value oscillates, which is interpreted as oscillation from the resonance frequency of the testbench. In this scenario, the driver's desired torque is constant during the gear shift process as in the conventional gear shift trajectories. As shown in the conventional gear shift trajectories of Fig. 2, the motor torque in the torque phase is constant. On the other hand, Fig. 7 shows that the motor torque is controlled actively in the torque phase to alleviate the torque dip phenomenon of the output shaft. In the inertia phase, the shape of the proposed torque trajectories are similar to that of the conventional gear shift trajectories. However, because the optimization with the driveline model has been performed, the magnitude of reduction of the motor torque and the timing of recovering the motor torque have accurate values. The measured clutch and output shaft torque in each figure does not completely match the trajectories. This is a limitation of feedforward control. It occurs due to the difference between the model and the plant. In the case of the motor torque trajectory, since feedback control is added in the inertia phase, the measured motor torques are slightly different from the trajectory. The slip error disappears as time goes by in Fig. 7a due to the effect of the slip controller. Additionally,

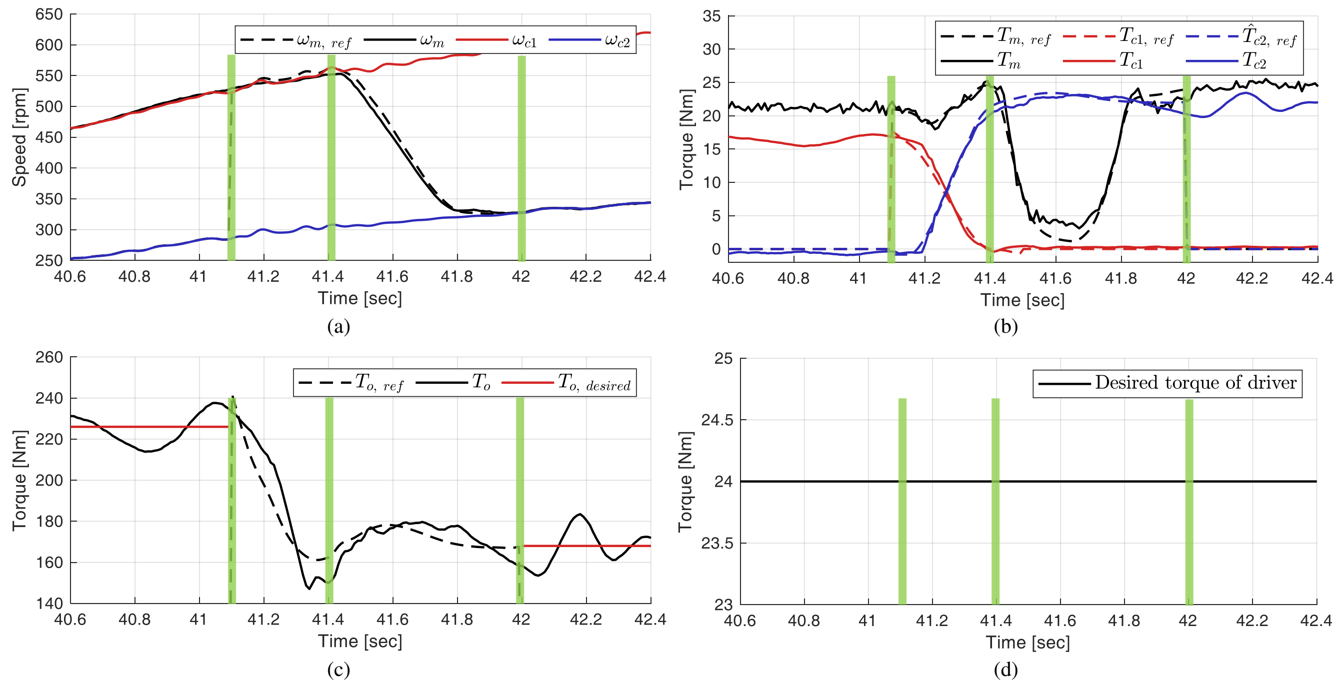

Fig. 7: Testbench experiments for scenario 1 : (a) Speed trajectory and measurements of each driveline component. (b) Torque trajectories and measurements of each driveline component. (c) Output shaft torque trajectory and measurements. (d) Driver's desired torque.

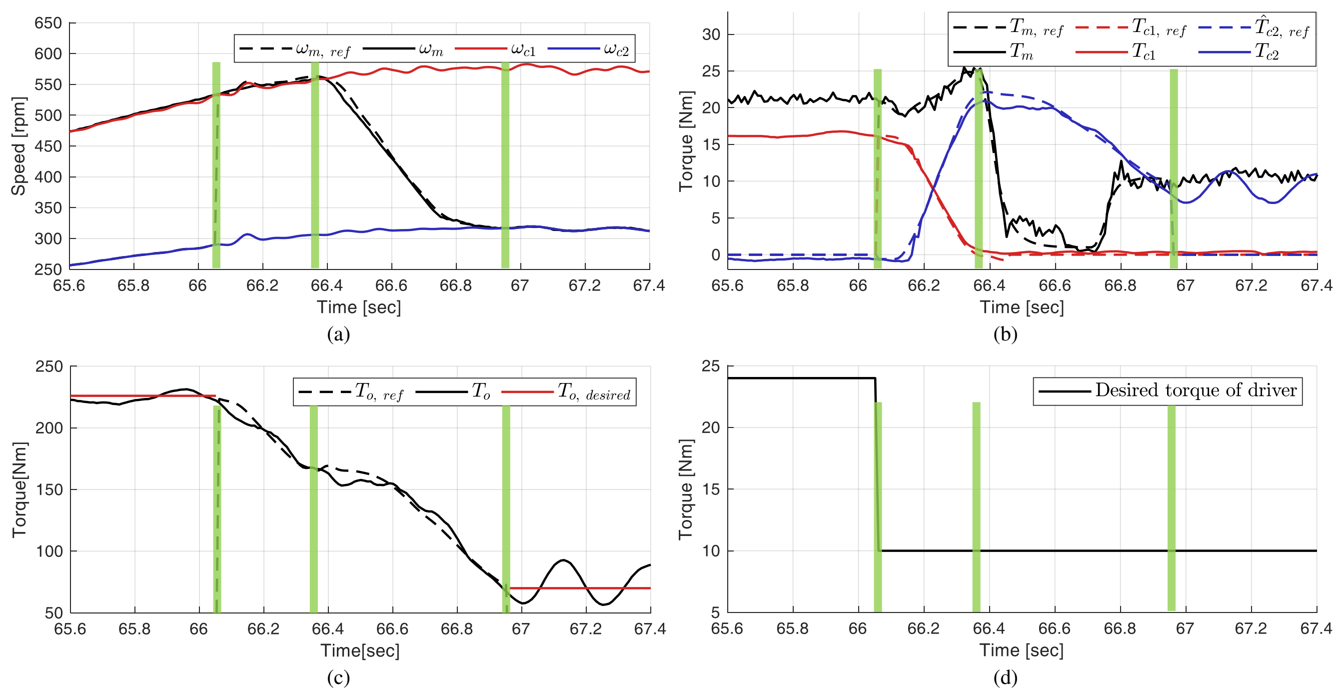

Fig. 8: Testbench experiments for scenario 2 : (a) Speed trajectory and measurements of each driveline component. (b) Torque trajectories and measurements of each driveline component. (c) Output shaft torque trajectory and measurements. (d) Driver's desired torque.

in Fig. 7c, the desired output torque value at each gear stage can be easily obtained by multiplying the gear ratio of each gear stage according to the pedal input of the driver in the 1st and 2nd gear situations. A solid red line indicates it in Fig. 7c. Here, it can be seen that the generated output torque trajectory is smoothly connected to the desired torque value at the end of the inertia phase. This result is because the output torque trajectory was generated considering the pedal input condition. As a result, it can be seen that a small lockup oscillation occurs in Fig. 7c.

Fig. 8 shows the experimental results for the second scenario. The torque phase is from 66.05 to $66.35s$, and the inertia phase is from 66.35 to $66.95s$. As the driver's pedal is released, the desired output torque value at the end of the gear shift is lowered. It is represented by a solid red line in Fig. 8c. Since this condition is reflected, it has a very different shape from the conventional gear shift trajectory. Fig. 8c has a smoother output shaft torque trajectory compared to Fig. 7c. Additionally, it has the advantage that the driver can obtain the desired torque value immediately after gear shifting. In other words, it means quick recovery of drivability in the gear shift process. In addition, it can be seen that a small lockup oscillation occurs in Fig. 8c. Furthermore, the trajectories satisfy all of the torque and jerk constraints in Fig. 8b. Due to the feedback control of the motor in the inertia phase, the shape of measured motor torque is slightly different from the trajectory in Fig. 8b.

Fig. 9 shows the experimental results of two cases for the third scenario. The first case (solid line) is the proposed algorithm to optimizie gear shift trajectories in real-time. It can cope with the variation of driver's pedal input. The second (dash-single dotted line) is a case for comparison without considering the change of driver's pedal input. In the second case, the driver's pedal input was applied to the motor torque after the gear shift process was completed. The measured values during the testbench experiment are plotted in both cases. Fig. 9a shows measured slip for both cases, Fig. 9b is measured torques of each driveline component for both cases, Fig. 9c shows measured output shaft torque for both cases, and Fig. 9d represents desired torque of driver for both cases. The torque phase is from 15.05 to $15.35s$, and the inertia phase is 15.35 to $15.95s$. In both cases, the torque limit and jerk limit conditions are not exceeded during the torque and inertia phases. However, in the case of the dash-single dotted line in Fig. 9c, the output torque value at the end of gear shifting indicates a different value from the desired output torque. Additional motor torque is suddenly applied after gear shifting to meet the driver's demand. Due to this, a large oscillation occurs in the output shaft torque in the comparison case. On the other hand, in the case of the solid line, it is controlled to a similar value with the desired output torque at the end of the gear shifting. For this reason, the solid line has little oscillation in Fig. 9c. The maximum jerk values that occurred in the corresponding period are measured as $0.87m/s^3$ in the proposed method and $3.42m/s^3$ in the comparison method. A jerk greater than $3m/s^3$ causes the driver to feel the vibration to some extent [29], resulting in poor ride comfort in the comparison case. It is because the gear shift control was performed in which the driver's pedal input change was not reflected in real-time. Thus, the driver feels the jerks after gear shifting, making the driver uncomfortable. On the other hand, since the proposed algorithm reflected the driver's pedal input in advance, it could provide a comfortable ride feeling to the driver during the gear shift process. In addition, the drivability is quickly recovered in the proposed method. In the case of the proposed method, the desired output torque could be obtained more than $0.4s$ faster than the conventional method during the gear shifting process in this scenario. From the above experimental results, the proposed trajectory can obtain fast output torque response (improvement of drivability) compared to the conventional trajectory when the pedal input is changed during gear shifting. Also, the proposed trajectory can provide a comfortable ride because jerk occurs very little during and after gear shifting. On the other hand, another way to reduce the oscillation of the comparison case in Fig. 9c is to increase the motor torque slowly after gear shift. However, in this case, the time to reach the desired motor torque after gear shift is increased. Thus, there is an additional loss in terms of drivability.

Tab. III summarizes the maximum torque and maximum

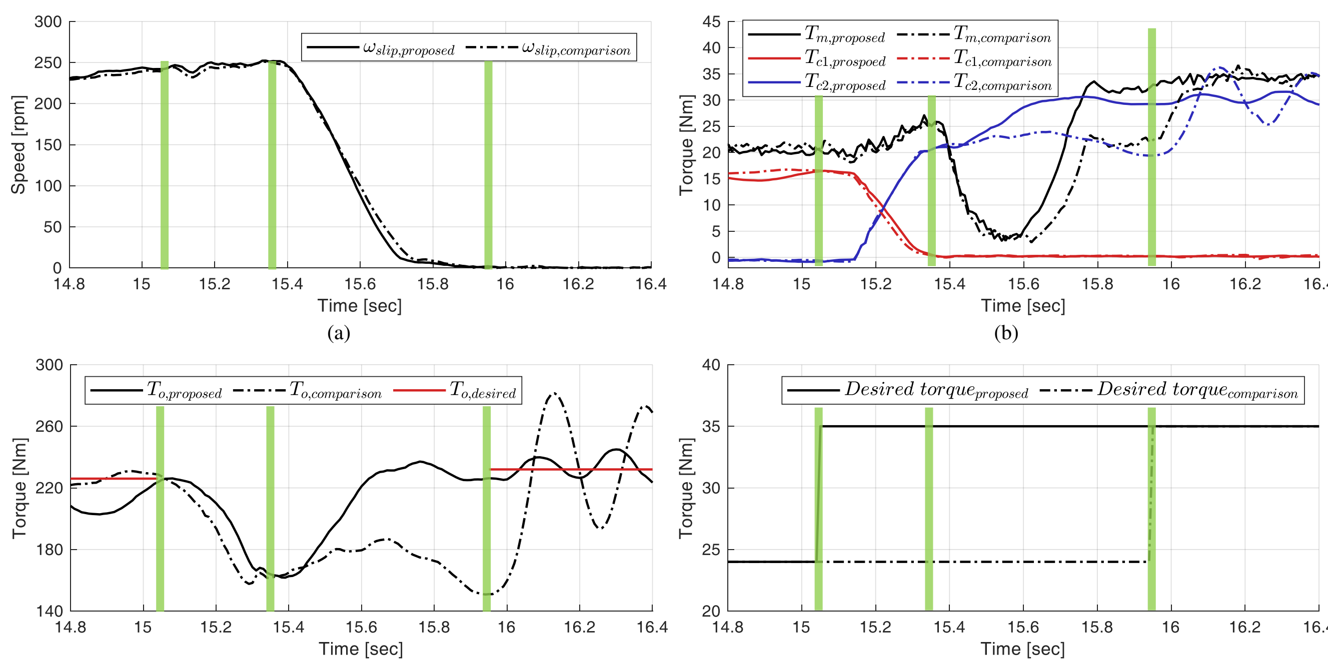

Fig. 9: Testbench experiments of the proposed algorithm and comparison for scenario 3 : (a) Measured slip for both cases. (b) Measured torques of each driveline component for both cases. (c) Measured output shaft torque for both cases. (d) Driver's desired torque for both cases.

TABLE III: Analysis of the gear shift trajectories for three scenarios

	Scenario 1	**Scenario 2**	**Scenario 3**
$T_{m,cmd,min}$	1	1	1
$T_{m,cmd,max}$	27.0	26.1	37.3
$T_{c2,cmd,max}$	23.4	22.1	31.9
$\dot{T}_{m,cmd,\max}$	264	237	263
$\dot{T}_{c2,cmd,\max}$	120	120	120
$jerk_{max}$	0.46	0.38	0.55

torque rate of the gear shift trajectories for the above three scenarios. In Tab. III, it can be seen that the proposed gear shift trajectories always satisfy the constraint conditions. In particular, the minimum value of motor torque and the maximum value of the clutch 2 torque rate stay at the bound of the constraints at some point. If we generate gear shift trajectories that do not consider constraints, there will inevitably be a problem of exceeding the constraints. In this case, the gear shift trajectories are generated that the lower-level controller cannot track. This shows why the gear shift trajectory must be made considering the lower-level controller limits. In addition, it is verified that the proposed optimization algorithm can respond to various situations in real-time such as scenarios 1, 2, and 3.

V. Conclusion

A real-time optimization algorithm for a gear shift trajectory using quadratic programming in electric vehicles was proposed. The driveline model and lower-level controller are arranged in a state-space form for each gear shift process. The trajectories with less shift shock while considering lower-level controller bandwidth were generated by setting the frequency-shaped jerk as an objective function. In addition, equality constraints were set for smooth model changes during the gear shift process. By setting the driver's pedal input as a boundary condition of the inertia phase, the drivability was recovered immediately after gear shift. Moreover, the maximum jerk and torque limit constraints were expressed as inequality constraints. Since the model and constraints are linear, the problem could be solved in real-time using quadratic programming. A real-time algorithm for generating a gear shift trajectory and feedforward input using the optimal solution was presented. Its real-time operation and performance were verified through testbench experiments. The results of this paper can be utilized to generate gear shift trajectories in various gear shift situations. In addition, different shapes of gear shift trajectories can be generated by changing the objective function. It is expected to be adopted to other gear shift logics in combination with the existing lower-level controller. Moreover, it can be easily extended to generate gear shift trajectories in parallel hybrid vehicles with DCT.

Acknowledgment

This research was partly supported by the BK21 FOUR Program of the National Research Foundation Korea (NRF) grant funded by the Ministry of Education (MOE), the Technology Innovation Program (20010263, Development of innovative design for UX environment improvement and commercialization model of wheelchair electric motorization kit with enhanced portability and convenience) funded By the Ministry of Trade, Industry & Energy (MOTIE, Korea), the National Research Foundation of Korea (NRF) grant funded by the Korea government (MSIP) (No. 2020R1A2B5B01001531), and the Technology Innovation Program (20014983, Development of autonomous chassis platform for a modular vehicle) funded By the Ministry of Trade, Industry & Energy (MOTIE, Korea).

VI. Appendix

A. Matrices of (11)

$$A_1 = A_{TP} = \begin{bmatrix} 0 & 0 & \frac{-(i_1-i_2)}{(J_m i_1^2+J_{o,eq})\eta} & \frac{(i_1-i_2)i_1}{(J_m i_1^2+J_{o,eq})} & 0 & \frac{-(i_1-i_2)^2}{(J_m i_1^2+J_{o,eq})} & 0 & 0 \\ 0 & 0 & -\left(\frac{1}{(J_m i_1^2+J_{o,eq})\eta}+\frac{1}{Jv}\right) & \frac{i_1}{(J_m i_1^2+J_{o,eq})} & 0 & \frac{-(i_1-i_2)}{(J_m i_1^2+J_{o,eq})} & 0 & \frac{1}{J_v} \\ 0 & k_{o,eq} & -c_{o,eq}\left(\frac{1}{(J_m i_1^2+J_{o,eq})\eta}+\frac{1}{Jv}\right) & \frac{c_{o,eq} i_1}{(J_m i_1^2+J_{o,eq})} & 0 & \frac{-c_{o,eq}(i_1-i_2)}{(J_m i_1^2+J_{o,eq})} & 0 & \frac{c_{o,eq}}{J_v} \\ 0 & 0 & 0 & -a_1 & a_1 & 0 & 0 & 0 \\ 0 & 0 & 0 & 0 & 0 & 0 & 0 & 0 \\ 0 & 0 & 0 & 0 & 0 & -a_2 & a_2 & 0 \\ 0 & 0 & 0 & 0 & 0 & 0 & 0 & 0 \\ 0 & 0 & 0 & 0 & 0 & 0 & 0 & 0 \end{bmatrix}$$

$$A_{IP} = \begin{bmatrix} 0 & 0 & \frac{i_2}{J_{o,eq}\eta} & \frac{1}{J_m} & 0 & -\left(\frac{1}{J_m}+\frac{i_2^2}{J_{o,eq}}\right) & 0 & 0 \\ 0 & 0 & -\left(\frac{1}{J_{o,eq}\eta}+\frac{1}{J_v}\right) & 0 & 0 & \frac{i_2}{J_{o,eq}} & 0 & \frac{1}{J_v} \\ 0 & k_{o,eq} & -c_{o,eq}\left(\frac{1}{J_{o,eq}\eta}+\frac{1}{J_v}\right) & 0 & 0 & \frac{c_{o,eq} i_2}{J_{o,eq}} & 0 & \frac{c_{o,eq}}{J_v} \\ 0 & 0 & 0 & -a_1 & a_1 & 0 & 0 & 0 \\ 0 & 0 & 0 & 0 & 0 & 0 & 0 & 0 \\ 0 & 0 & 0 & 0 & 0 & -a_2 & a_2 & 0 \\ 0 & 0 & 0 & 0 & 0 & 0 & 0 & 0 \\ 0 & 0 & 0 & 0 & 0 & 0 & 0 & 0 \end{bmatrix}$$

$$A_2 = \begin{bmatrix} 0 & 0 & 0 & 0 & 0 & 0 & 0 & 0 \\ 0 & 0 & -\left(\frac{1}{(J_m i_2^2+J_{o,eq})\eta}+\frac{1}{Jv}\right) & \frac{i_2}{(J_m i_2^2+J_{o,eq})} & 0 & 0 & 0 & \frac{1}{J_v} \\ 0 & k_{o,eq} & -c_{o,eq}\left(\frac{1}{(J_m i_2^2+J_{o,eq})\eta}+\frac{1}{Jv}\right) & \frac{c_{o,eq} i_2}{(J_m i_2^2+J_{o,eq})} & 0 & 0 & 0 & \frac{c_{o,eq}}{J_v} \\ 0 & 0 & 0 & -a_1 & a_1 & 0 & 0 & 0 \\ 0 & 0 & 0 & 0 & 0 & 0 & 0 & 0 \\ 0 & 0 & 0 & 0 & 0 & -a_2 & a_2 & 0 \\ 0 & 0 & 0 & 0 & 0 & 0 & 0 & 0 \\ 0 & 0 & 0 & 0 & 0 & 0 & 0 & 0 \end{bmatrix}, \; B_{TP} = B_{IP} = \begin{bmatrix} 0 & 0 \\ 0 & 0 \\ 0 & 0 \\ 0 & 0 \\ 1 & 0 \\ 0 & 0 \\ 0 & 1 \\ 0 & 0 \end{bmatrix}$$

References

[1] BloombergNEF, "Electric vehicle outlook 2019," BloombergNEF, May. 15, 2019. [Online], available : https://legacy-assets.eenews.net/open_files/assets/2019/05/15/document_ew_02.pdf.

[2] M. R. Ahssan, M. M. Ektesabi, and S. A. Gorji, "Electric vehicle with multi-speed transmission: a review on performances and complexities," SAE International Journal of Alternative Powertrains, vol. 7, no. 2, pp. 169–182, 2018.

[3] G. Wu, X. Zhang, and Z. Dong, Impacts of two-speed gearbox on electric vehicle's fuel economy and performance. SAE International Warrendale, PA, USA, 2013, vol. 2.

[4] J. Ruan, P. Walker, and N. Zhang, "A comparative study energy consumption and costs of battery electric vehicle transmissions," Applied Energy, vol. 165, pp. 119–134, 2016.

[5] Q. Ren, D. Crolla, and A. Morris, "Effect of transmission design on electric vehicle (ev) performance," in 2009 IEEE vehicle power and propulsion conference. IEEE, 2009, pp. 1260–1265.

[6] T. Hofman and C. Dai, "Energy efficiency analysis and comparison of transmission technologies for an electric vehicle," in 2010 IEEE vehicle power and propulsion conference. IEEE, 2010, pp. 1–6.

[7] P. D. Walker and N. Zhang, "Modelling of dual clutch transmission equipped powertrains for shift transient simulations," Mechanism and Machine Theory, vol. 60, pp. 47–59, 2013.

[8] M. Kulkarni, T. Shim, and Y. Zhang, "Shift dynamics and control of dual-clutch transmissions," Mechanism and machine theory, vol. 42, no. 2, pp. 168–182, 2007.

[9] B. Z. Gao, H. Chen, K. Sanada, and Y. Hu, "Design of clutch-slip controller for automatic transmission using backstepping," IEEE/ASME Transactions on mechatronics, vol. 16, no. 3, pp. 498–508, 2010.

[10] J. M. Maguire, Dynamic analysis and control system design of automatic transmissions. SAE International, 2013.

[11] M. Goetz, M. Levesley, and D. Crolla, "Dynamics and control of gearshifts on twin-clutch transmissions," Proceedings of the institution of mechanical engineers, Part D: Journal of Automobile Engineering, vol. 219, no. 8, pp. 951–963, 2005.

[12] S. Kim and S. B. Choi, "Cooperative control of drive motor and clutch for gear shift of hybrid electric vehicles with dual-clutch transmission," IEEE/ASME Transactions on Mechatronics, vol. 25, no. 3, pp. 1578–1588, 2020.

[13] S. Kahlbau and D. Bestle, "Optimal shift control for automatic transmission#," Mechanics Based Design of Structures and Machines, vol. 41, no. 3, pp. 259–273, 2013.

[14] L. Glielmo, L. Iannelli, V. Vacca, and F. Vasca, "Gearshift control for automated manual transmissions," IEEE/ASME transactions on mechatronics, vol. 11, no. 1, pp. 17–26, 2006.

[15] A. Haj-Fraj and F. Pfeiffer, "Optimal control of gear shift operations in automatic transmissions," Journal of the Franklin Institute, vol. 338, no. 2-3, pp. 371–390, 2001.

[16] S. Kim, J. Oh, and S. Choi, "Gear shift control of a dual-clutch transmission using optimal control allocation," Mechanism and Machine Theory, vol. 113, pp. 109–125, 2017.

[17] B. Gao, Y. Xiang, H. Chen, Q. Liang, and L. Guo, "Optimal trajectory planning of motor torque and clutch slip speed for gear shift of a two-

speed electric vehicle," Journal of Dynamic Systems, Measurement, and Control, vol. 137, no. 6, p. 061016, 2015.
[18] G. Li and D. Görges, "Optimal control of the gear shifting process for shift smoothness in dual-clutch transmissions," Mechanical Systems and Signal Processing, vol. 103, pp. 23–38, 2018.
[19] J. Park and S. Choi, "Gear shifting based on mimo model predictive control for convenient adjustment of shifting performance," IEEE Transactions on Vehicular Technology, vol. 71, no. 1, pp. 233–249, 2021.
[20] X. Lu, H. Chen, B. Gao, Z. Zhang, and W. Jin, "Data-driven predictive gearshift control for dual-clutch transmissions and fpga implementation," IEEE Transactions on Industrial Electronics, vol. 62, no. 1, pp. 599–610, 2014.
[21] K. Zhao, Z. Li, Y. Chen, and Y. Liu, "Multi-objective optimization of gearshift trajectory planning for multi-speed electric vehicles," Engineering Optimization, pp. 1–24, 2021.
[22] T. Lee, D.-H. Kim, and S. B. Choi, "Driveline modeling with transmission loss and robust torque observer design for dual clutch transmission," IEEE Transactions on Vehicular Technology, vol. 71, no. 2, pp. 1267–1279, 2021.
[23] J. J. Oh, S. B. Choi, and J. Kim, "Driveline modeling and estimation of individual clutch torque during gear shifts for dual clutch transmission," Mechatronics, vol. 24, no. 5, pp. 449–463, 2014.
[24] J. J. Oh and S. B. Choi, "Real-time estimation of transmitted torque on each clutch for ground vehicles with dual clutch transmission," IEEE/ASME Transactions on Mechatronics, vol. 20, no. 1, pp. 24–36, 2014.
[25] S. Kim and S. Choi, "Control-oriented modeling and torque estimations for vehicle driveline with dual-clutch transmission," Mechanism and Machine Theory, vol. 121, pp. 633–649, 2018.
[26] J. Kim, "Real-time torque estimation of automotive powertrain with dual-clutch transmissions," IEEE Transactions on Control Systems Technology, 2022.
[27] E. F. Camacho and C. B. Alba, Model predictive control. Springer science & business media, 2013.
[28] L. Wang, Model predictive control system design and implementation using MATLAB®. Springer Science & Business Media, 2009.
[29] Q. Huang and H. Wang, "Fundamental study of jerk: evaluation of shift quality and ride comfort," SAE Technical Paper, Tech. Rep., 2004.
[30] L. L. Hoberock, "A survey of longitudinal acceleration comfort studies in ground transportation vehicles," Council for Advanced Transportation Studies, Tech. Rep., 1976.
[31] H. J. Ferreau, C. Kirches, A. Potschka, H. G. Bock, and M. Diehl, "qpoases: A parametric active-set algorithm for quadratic programming," Mathematical Programming Computation, vol. 6, no. 4, pp. 327–363, 2014.
[32] H. J. Ferreau, H. G. Bock, and M. Diehl, "An online active set strategy to overcome the limitations of explicit mpc," International Journal of Robust and Nonlinear Control: IFAC-Affiliated Journal, vol. 18, no. 8, pp. 816–830, 2008.

Taeheon Lee received his B.S. and M.S. degrees in mechanical engineering from Korea Advanced Institute of Science and Technology (KAIST), Daejeon, Korea, where he is currently working toward his Ph.D. degree. His research interests include powertrain modeling and control, vehicle powertrain, vehicle dynamics and control, and control and optimization theory.

Seibum.B.Choi received B.S. degree in mechanical engineering from Seoul National University, Korea, M.S. degree in mechanical engineering from Korea Advanced Institute of Science and Technology (KAIST), Korea, and the Ph.D. degree in controls from the University of California, Berkeley in 1993. Since 2006, he has been with the faculty of the Mechanical Engineering department at KAIST. His research interests include fuel saving technology, vehicle dynamics and control, and application of self-energizing mechanism.